





Research Article

An Efficient Iterative Algorithm for Solving the Split Feasibility Problem in Hilbert Spaces Applicable in Image Deblurring, Signal Recovering, and Polynomiography

Lanchakorn Kittiratanawasin ¹, Damrongsak Yambangwai ²,
Chonjaroen Chairatsiripong ² and Tanakit Thianwan ²

¹Department of Mathematics, Faculty of Science, Kasetsart University, Bangkok 10900, Thailand

²Department of Mathematics, School of Science, University of Phayao, Phayao 56000, Thailand

Correspondence should be addressed to Tanakit Thianwan; tanakit.th@up.ac.th

Received 15 November 2022; Revised 23 December 2022; Accepted 28 March 2023; Published 22 April 2023

Academic Editor: Kenan Yildirim

Copyright © 2023 Lanchakorn Kittiratanawasin et al. This is an open access article distributed under the Creative Commons Attribution License, which permits unrestricted use, distribution, and reproduction in any medium, provided the original work is properly cited.

The split feasibility problem (SFP) in Hilbert spaces is addressed in this study using an efficient iterative approach. Under mild conditions, we prove convergence theorems for the algorithm for finding a solution to the SFP. We also present numerical examples to illustrate that the acceleration of our algorithm is effective. Our results are applied to solve image deblurring and signal recovery problems. Furthermore, we show the use of the proposed method to generate polynomiographs.

1. Introduction

Let \mathcal{C} and \mathcal{Q} be nonempty closed convex subsets of real Hilbert spaces \mathcal{H}_1 and \mathcal{H}_2 , respectively. The split feasibility problem (SFP for short) can be formulated as finding a point u^* in \mathcal{C} with the property

$$\mathcal{A}u^* \in \mathcal{Q}, \quad (1)$$

where $\mathcal{A}: \mathcal{H}_1 \rightarrow \mathcal{H}_2$ is a bounded linear operator.

For modeling inverse problems, Censor and Elfving [1] proposed the SFP in finite-dimensional Hilbert spaces. Later on, the SFP can also be applied to medical image reconstruction and signal processing; see, e.g., [2–10].

The SFP (1) can be written as a fixed point problem by using

$$\mathcal{P}_{\mathcal{C}}[\mathcal{I} - \gamma\mathcal{A}^*(\mathcal{I} - \mathcal{P}_{\mathcal{Q}})\mathcal{A}]u^* = u^*, \quad (2)$$

where $\mathcal{P}_{\mathcal{C}}$ and $\mathcal{P}_{\mathcal{Q}}$ are the (orthogonal) projections onto \mathcal{C} and \mathcal{Q} , respectively, $\gamma > 0$ is any positive constant, and \mathcal{A}^* denotes the adjoint of \mathcal{A} . That is, u^* solves the SFP (1) if and only if u^* solves the fixed point equation (2) (see [11]). For

more effective, the readers can see [8, 12–22]. In [7], Byrne proposed the $\mathcal{C}\mathcal{Q}$ algorithm by

$$u_{k+1} = \mathcal{P}_{\mathcal{C}}[\mathcal{I} - \gamma\mathcal{A}^*(\mathcal{I} - \mathcal{P}_{\mathcal{Q}})\mathcal{A}]u_k, k \geq 0, \quad (3)$$

where $0 < \gamma < 2/\|\mathcal{A}\|^2$, $\mathcal{A}^*: \mathcal{H}_2 \rightarrow \mathcal{H}_1$ is the adjoint of \mathcal{A} , and $\mathcal{P}_{\mathcal{C}}$ and $\mathcal{P}_{\mathcal{Q}}$ are the projections onto \mathcal{C} and \mathcal{Q} , respectively. The $\mathcal{C}\mathcal{Q}$ -algorithm (3) has been a useful instrument for solving the SFP due to its own virtues-simple computation, and many variants of the $\mathcal{C}\mathcal{Q}$ -algorithm have been employed in several literature, such as [8, 9], and so on.

The three-step procedures were first introduced by Noor [23]. This method is applied to many problems. For example, see [24–26].

Recently, the following three step iteration method used to solve the SFP was defined by Dang and Gao [27]:

$$\begin{aligned} w_n &= (1 - \gamma_n)u_n + \gamma_n\mathcal{P}_{\mathcal{C}}[(1 - \lambda_n)\mathcal{U}]u_n, \\ \varsigma_n &= (1 - \beta_n)u_n + \beta_n\mathcal{P}_{\mathcal{C}}[(1 - \lambda_n)\mathcal{U}]w_n, \\ u_{n+1} &= (1 - \alpha_n)u_n + \alpha_n\mathcal{P}_{\mathcal{C}}[(1 - \lambda_n)\mathcal{U}]\varsigma_n, \end{aligned} \quad (4)$$

where $\mathcal{U} = \mathcal{F} - \gamma\mathcal{A}^*(\mathcal{F} - \mathcal{P}_{\mathcal{Q}})\mathcal{A}$ and $\{\alpha_n\}, \{\beta_n\}, \{\gamma_n\}, \{\lambda_n\}$ are real sequences in $(0, 1)$. Strong convergence theorems are studied for (4) under some parametric controlling conditions. In addition, Thakur et al. [28] proposed the new three-step iterative method for solving fixed points of nonexpansive mapping.

Motivated by Dang et al., we propose an efficient iterative method which generates a sequence $\{u_n\}$ by

$$\begin{aligned} w_n &= (1 - \gamma_n)u_n + \gamma_n\mathcal{T}u_n, \\ \varsigma_n &= (1 - \beta_n)w_n + \beta_n\mathcal{T}w_n, \\ u_{n+1} &= (1 - \alpha_n)\mathcal{T}u_n + \alpha_n\mathcal{T}\varsigma_n, \end{aligned} \quad (5)$$

where $\mathcal{T} = \mathcal{P}_{\mathcal{E}}[\mathcal{F} - \gamma\mathcal{A}^*(\mathcal{F} - \mathcal{P}_{\mathcal{Q}})\mathcal{A}]$ and $\{\alpha_n\}, \{\beta_n\}, \{\gamma_n\}$ are real sequences in $(0, 1)$.

2. Preliminaries

Let \mathcal{H} be a real Hilbert space with inner product $\langle \cdot, \cdot \rangle$ and induce norm $\|\cdot\|$. I denotes the identity operator in \mathcal{H} . We will denote the set of fixed points of: $\mathcal{H} \rightarrow \mathcal{H}$ by $F(\mathcal{T}) = \{u \in \mathcal{H} : \mathcal{T}u = u\}$. For the sequence $\{u_n\}$ to u in \mathcal{H} , the strong convergence and the weak convergence are denoted by $u_n \rightarrow u$ and $u_n \rightharpoonup u$, respectively. An operator \mathcal{T} on \mathcal{H} is nonexpansive if, for each $u, v \in \mathcal{H}$,

$$\|\mathcal{T}u - \mathcal{T}v\| \leq \|u - v\|, \quad (6)$$

\mathcal{T} is said to be λ -Lipschitz continuous, if each $u, v \in \mathcal{H}$, we have

$$\|\mathcal{T}u - \mathcal{T}v\| \leq \lambda\|u - v\|, \quad (7)$$

for a constant $\lambda > 0$. Assume $\varphi > 0$. Then, \mathcal{T} is called φ -inverse strongly monotone (φ -ism), if each $u, v \in \mathcal{H}$, we have

$$\langle u - v, \mathcal{T}u - \mathcal{T}v \rangle \geq \varphi\|\mathcal{T}u - \mathcal{T}v\|^2. \quad (8)$$

Recall that 1-ism \mathcal{T} is also known as being firmly nonexpansive, that is, for each $u, v \in \mathcal{H}$,

$$\langle u - v, \mathcal{T}u - \mathcal{T}v \rangle \geq \|\mathcal{T}u - \mathcal{T}v\|^2. \quad (9)$$

Let the solution set $\Omega = \{u \in \mathcal{C} : \mathcal{A}u \in \mathcal{Q}\} = \mathcal{C} \cap \mathcal{A}^{-1}\mathcal{Q}$ of the SFP (1) be a closed, convex, and nonempty set. Let $\mathcal{P}_{\mathcal{E}}$ denote the projection from \mathcal{H} onto a nonempty closed convex subset \mathcal{E} of \mathcal{H} that is, $\mathcal{P}_{\mathcal{E}}(u) := \operatorname{argmin}_{v \in \mathcal{E}} \|u - v\|$. Suppose that $d(u, \mathcal{E}) := \inf\{\|u - v\| : v \in \mathcal{E}\}$. We have the following important lemma due to Feng et al. [29]:

Lemma 1. *If $\mathcal{T} = \mathcal{P}_{\mathcal{E}}[\mathcal{F} - \gamma\mathcal{A}^*(\mathcal{F} - \mathcal{P}_{\mathcal{Q}})\mathcal{A}]$, where $0 < \gamma < 2/\|\mathcal{A}\|^2$, then \mathcal{T} is a nonexpansive map.*

Lemma 2 (see [30]). *Let $\{u_n\}$ be a sequence of Hilbert space \mathcal{H} . If $\{u_n\}$ converges weakly to u , then for any $v \in \mathcal{H}$ and $v \neq u$, we have $\lim_{n \rightarrow \infty} \inf\|u_n - u\| < \lim_{n \rightarrow \infty} \inf\|u_n - v\|$.*

Lemma 3 (see [30]). *Let \mathcal{C} be a closed, convex, and nonempty subset of real Hilbert space \mathcal{H} , and $\mathcal{T} : \mathcal{C} \rightarrow \mathcal{C}$ be*

a nonexpansive mapping. Then, $\mathcal{F} - \mathcal{T}$ is demiclosed at zero, i.e., if $u_n \rightharpoonup u \in \mathcal{C}$ and $u_n - \mathcal{T}u_n \rightarrow 0$, then $u = \mathcal{T}u$.

Lemma 4 (see [31]). *Let X be a uniformly convex Banach space and $0 < p \leq t_n \leq q < 1$ for all $n \in \mathbb{N}$. Let $\{u_n\}$ and $\{v_n\}$ be two sequences of X such that $\limsup_{n \rightarrow \infty} \|u_n\| \leq r$, $\limsup_{n \rightarrow \infty} \|v_n\| \leq r$ and $\limsup_{n \rightarrow \infty} \|t_n u_n + (1 - t_n)v_n\| = r$ hold for some $r \geq 0$. Then, $\limsup_{n \rightarrow \infty} \|u_n - v_n\| = 0$.*

3. Convergence Results

Lemma 5. *Let $\{u_n\}$ be generated by (5) and $\mathcal{T} = \mathcal{P}_{\mathcal{E}}[\mathcal{F} - \gamma\mathcal{A}^*(\mathcal{F} - \mathcal{P}_{\mathcal{Q}})\mathcal{A}]$. Then, $\lim_{n \rightarrow \infty} \|u_n - u^*\|$ exists for any $u^* \in F(\mathcal{T})$.*

Proof. Given $u^* \in F(\mathcal{T})$. By nonexpansiveness of \mathcal{T} and using (5), we have

$$\begin{aligned} \|w_n - u^*\| &= \|(1 - \gamma_n)u_n + \gamma_n\mathcal{T}u_n - u^*\| \\ &\leq (1 - \gamma_n)\|u_n - u^*\| + \gamma_n\|\mathcal{T}u_n - u^*\| \\ &\leq (1 - \gamma_n)\|u_n - u^*\| + \gamma_n\|u_n - u^*\| \\ &= \|u_n - u^*\|, \end{aligned} \quad (10)$$

and so

$$\begin{aligned} \|\varsigma_n - u^*\| &= \|(1 - \beta_n)w_n + \beta_n\mathcal{T}w_n - u^*\| \\ &\leq (1 - \beta_n)\|w_n - u^*\| + \beta_n\|\mathcal{T}w_n - u^*\| \\ &\leq (1 - \beta_n)\|w_n - u^*\| + \beta_n\|w_n - u^*\| \\ &= \|w_n - u^*\| \\ &\leq \|u_n - u^*\|. \end{aligned} \quad (11)$$

Using (10) and (11), we have

$$\begin{aligned} \|u_{n+1} - u^*\| &= \|(1 - \alpha_n)\mathcal{T}u_n + \alpha_n\mathcal{T}\varsigma_n - u^*\| \\ &\leq (1 - \alpha_n)\|\mathcal{T}u_n - u^*\| + \alpha_n\|\mathcal{T}\varsigma_n - u^*\| \\ &\leq (1 - \alpha_n)\|u_n - u^*\| + \alpha_n\|\varsigma_n - u^*\| \\ &\leq (1 - \alpha_n)\|u_n - u^*\| + \alpha_n\|u_n - u^*\| \\ &= \|u_n - u^*\|. \end{aligned} \quad (12)$$

Since u^* is chosen arbitrarily in $F(\mathcal{T})$, one deduces that $\{\|u_n - u^*\|\}_n$ is decreasing. It follows that $\lim_{n \rightarrow \infty} \|u_n - u^*\|$ exists for any $u^* \in F(\mathcal{T})$. This completes the proof. \square

Lemma 6. *Let $\{u_n\}$ be generated by (5). and $\mathcal{T} = \mathcal{P}_{\mathcal{E}}[\mathcal{F} - \gamma\mathcal{A}^*(\mathcal{F} - \mathcal{P}_{\mathcal{Q}})\mathcal{A}]$. Then, $\lim_{n \rightarrow \infty} \|u_n - \mathcal{T}u_n\| = 0$.*

Proof. By Lemma 5, we see that $\lim_{n \rightarrow \infty} \|u_n - u^*\|$ exists for any $u^* \in F(\mathcal{T})$. Assume that

$$\lim_{n \rightarrow \infty} \|u_n - u^*\| = c. \quad (13)$$

We take the lim sup of (10) and (11), and we get

$$\limsup_{n \rightarrow \infty} \|w_n - u^*\| \leq c, \tag{14}$$

and

$$\limsup_{n \rightarrow \infty} \|\zeta_n - u^*\| \leq c. \tag{15}$$

In addition, by nonexpensiveness of \mathcal{T} , we have

$$\begin{aligned} \|\mathcal{T}u_n - u^*\| &\leq \|u_n - u^*\|, \|\mathcal{T}w_n - u^*\| \\ &\leq \|w_n - u^*\|, \|\mathcal{T}\zeta_n - u^*\| \leq \|\zeta_n - u^*\|. \end{aligned} \tag{16}$$

Again, by taking the lim sup on both sides, we get

$$\limsup_{n \rightarrow \infty} \|\mathcal{T}u_n - u^*\| \leq c, \tag{17}$$

$$\limsup_{n \rightarrow \infty} \|\mathcal{T}w_n - u^*\| \leq c, \tag{18}$$

and

$$\limsup_{n \rightarrow \infty} \|\mathcal{T}\zeta_n - u^*\| \leq c. \tag{19}$$

In addition,

$$\begin{aligned} c &= \lim_{n \rightarrow \infty} \|u_{n+1} - u^*\| \\ &= \lim_{n \rightarrow \infty} \|(1 - \alpha_n)(\mathcal{T}u_n - u^*) - \alpha_n(\mathcal{T}\zeta_n - u^*)\|. \end{aligned} \tag{20}$$

Using (17)–(19) and Lemma 4, we have

$$\lim_{n \rightarrow \infty} \|\mathcal{T}u_n - \mathcal{T}\zeta_n\| = 0. \tag{21}$$

In addition,

$$\begin{aligned} \|u_{n+1} - u^*\| &= \|(1 - \alpha_n)(\mathcal{T}u_n - u^*) + \alpha_n(\mathcal{T}\zeta_n - u^*)\| \\ &\leq (1 - \alpha_n)\|\mathcal{T}u_n - u^*\| + \alpha_n\|\mathcal{T}\zeta_n - u^*\| \\ &\leq (1 - \alpha_n)\|\mathcal{T}u_n - u^*\| + \alpha_n\|\mathcal{T}u_n - \mathcal{T}\zeta_n\| \\ &\quad + \alpha_n\|\mathcal{T}u_n - u^*\| \\ &= \|\mathcal{T}u_n - u^*\| + \alpha_n\|\mathcal{T}\zeta_n - \mathcal{T}u_n\|, \end{aligned} \tag{22}$$

and taking the lim inf on both sides in this inequality, we have

$$c \leq \liminf_{n \rightarrow \infty} \|\mathcal{T}u_n - u^*\|. \tag{23}$$

Using (17) and (23), we have

$$\lim_{n \rightarrow \infty} \|\mathcal{T}u_n - u^*\| = c. \tag{24}$$

Since,

$$\begin{aligned} \|\mathcal{T}u_n - u^*\| &\leq \|\mathcal{T}u_n - \mathcal{T}\zeta_n\| + \|\mathcal{T}\zeta_n - u^*\| \\ &\leq \|\mathcal{T}u_n - \mathcal{T}\zeta_n\| + \|\zeta_n - u^*\|. \end{aligned} \tag{25}$$

Using (21) and (24) and take the lim inf of (25), and we get

$$c \leq \lim_{n \rightarrow \infty} \inf \|\zeta_n - u^*\|. \tag{26}$$

From (15) and (26), we get

$$\lim_{n \rightarrow \infty} \|\zeta_n - u^*\| = c. \tag{27}$$

In addition,

$$\begin{aligned} c &= \lim_{n \rightarrow \infty} \|\zeta_n - u^*\| \\ &= \lim_{n \rightarrow \infty} \|(1 - \beta_n)(w_n - u^*) + \beta_n(\mathcal{T}w_n - u^*)\|. \end{aligned} \tag{28}$$

By (14), (18), and (28) and Lemma 4, we have

$$\lim_{n \rightarrow \infty} \|\mathcal{T}w_n - w_n\| = 0. \tag{29}$$

In addition,

$$\begin{aligned} \|\zeta_n - u^*\| &= \|(1 - \beta_n)w_n + \beta_n\mathcal{T}w_n - u^*\| \\ &\leq (1 - \beta_n)\|w_n - u^*\| + \beta_n\|\mathcal{T}w_n - u^*\| \\ &\leq (1 - \beta_n)\|w_n - u^*\| + \beta_n\|\mathcal{T}w_n - w_n\| \\ &\quad + \beta_n\|w_n - u^*\| \\ &= \|w_n - u^*\| + \beta_n\|\mathcal{T}w_n - w_n\|. \end{aligned} \tag{30}$$

Using (27) and (29) and take the lim inf of (30), and we get

$$c \leq \liminf_{n \rightarrow \infty} \|w_n - u^*\|. \tag{31}$$

From (14) and (31), we get

$$\lim_{n \rightarrow \infty} \|w_n - u^*\| = c. \tag{32}$$

By using (32), we have

$$\begin{aligned} c &= \lim_{n \rightarrow \infty} \|w_n - u^*\| \\ &= \lim_{n \rightarrow \infty} \|(1 - \gamma_n)(u_n - u^*) + \gamma_n(\mathcal{T}u_n - u^*)\|. \end{aligned} \tag{33}$$

It follows from (13), (17), and (33) and Lemma 4 that

$$\lim_{n \rightarrow \infty} \|\mathcal{T}u_n - u_n\| = 0. \tag{34}$$

Additionally, the solution set, denoted by Ω , is the same as the fixed point set, denoted by \mathcal{F} , i.e., $\Omega = F(\mathcal{F}) = \mathcal{C} \cap \mathcal{A}^{-1}Q \neq \emptyset$ (see [11, 12]) for more details. \square

Theorem 1. *Let $\{u_n\}$ be generated (5) and $\mathcal{T} = \mathcal{P}_{\mathcal{C}}[\mathcal{F} - \gamma\mathcal{A}^*(\mathcal{F} - \mathcal{P}_{\mathcal{Q}})\mathcal{A}]$. Then, $\{u_n\}$ converges weakly to a point in Ω .*

Proof. Since $\Omega = F(\mathcal{F}) \neq \emptyset$. Then, we only need to show that the sequence $\{u_n\}$ converges weakly to a point in $F(\mathcal{F})$. Taking $u^* \in F(\mathcal{F})$, using Lemma 5, $\lim_{n \rightarrow \infty} \|u_n - u^*\|$ exists. We show that the subsequences of $\{u_n\}$ only have a weak limit in $F(\mathcal{F})$. Suppose that subsequences $\{u_{n_i}\}$ and $\{u_{n_j}\}$ of $\{u_n\}$ converge weakly to ξ and ζ , respectively. From Lemma 6, we have

$$\lim_{n \rightarrow \infty} \|u_{n_i} - \mathcal{T}u_{n_i}\| = 0 = \lim_{n \rightarrow \infty} \|u_{n_j} - \mathcal{T}u_{n_j}\|. \quad (35)$$

It follows from Lemma 3 that $\xi, \varsigma \in F(\mathcal{T})$. Next, we show that the weak limit is unique. Since $\mathcal{T} = \mathcal{P}_{\mathcal{E}}[\mathcal{F} - \gamma\mathcal{A}^*(\mathcal{F} - \mathcal{P}_{\mathcal{Q}})\mathcal{A}]$ is nonexpansive mapping. Using Lemma 5, we have $\lim_{n \rightarrow \infty} \|u_n - u^*\|$ exists. Suppose that $\xi \neq \varsigma$. Using Lemma 2, we have

$$\begin{aligned} \lim_{n \rightarrow \infty} \|u_n - \xi\| &= \lim_{n_i \rightarrow \infty} \|u_{n_i} - \xi\| < \lim_{n_i \rightarrow \infty} \|u_{n_i} - \varsigma\| \\ &= \lim_{n \rightarrow \infty} \|u_n - \varsigma\| = \lim_{n_j \rightarrow \infty} \|u_{n_j} - \varsigma\| \\ &< \lim_{n_j \rightarrow \infty} \|u_{n_j} - \xi\| = \lim_{n \rightarrow \infty} \|u_n - \xi\|. \end{aligned} \quad (36)$$

This is clearly contradictory, hence, $\xi = \varsigma$. Therefore, $\{u_n\}$ converges weakly to a point in $F(\mathcal{T})$. Thus the sequence $\{u_n\}$, converges weakly to a point in Ω .

Mapping \mathcal{T} in \mathcal{H} is called averaged if there exist $\alpha \in (0, 1)$ and a nonexpansive operator S such that $\mathcal{T} = (1 - \alpha)\mathcal{F} + \alpha S$. Set

$$q(u) := \frac{1}{2} \|((\mathcal{F} - \mathcal{P}_{\mathcal{Q}})\mathcal{T})u\|, u \in \mathcal{E}. \quad (37)$$

We consider

$$\text{find } \min_{u \in \mathcal{E}} q(u). \quad (38)$$

By [32], the gradient of q is $\nabla q = \mathcal{T}^*(\mathcal{F} - \mathcal{P}_{\mathcal{Q}})\mathcal{T}$, where \mathcal{T}^* is the adjoint of \mathcal{T} . Since $\mathcal{F} - \mathcal{P}_{\mathcal{Q}}$ is nonexpansive, it follows that ∇q is L -Lipschitzian with $L = \|\mathcal{T}\|^2$. Therefore, ∇q is $1/L$ -ism and for any $0 < \mu < 2/L$, $\mathcal{F} - \mu\nabla q$ is averaged. Therefore, the composition $\mathcal{P}_{\mathcal{E}}(\mathcal{F} - \mu\nabla q)$ is also averaged. Set $\mathcal{T} := \mathcal{P}_{\mathcal{E}}(\mathcal{F} - \mu\nabla q)$. Note that the solution set of SFP is $F(\mathcal{T})$. The following new three-step can be used to find solutions of SFP: \square

Theorem 2. Assume that SFP is consistent. Suppose $\{\alpha_n\}$, $\{\beta_n\}$ and $\{\gamma_n\}$ are sequences in $[\delta, 1 - \delta]$ for all $n \in \mathbb{N}$ and for some δ in $(0, 1)$. Let $\{u_n\}$ be a sequence in \mathcal{E} generated by

$$\begin{aligned} w_n &= (1 - \gamma_n)u_n + \gamma_n\mathcal{P}_{\mathcal{E}}(\mathcal{F} - \mu\nabla q)u_n, \\ \varsigma_n &= (1 - \beta_n)w_n + \beta_n\mathcal{P}_{\mathcal{E}}(\mathcal{F} - \mu\nabla q)w_n, \\ u_{n+1} &= (1 - \alpha_n)\mathcal{P}_{\mathcal{E}}(I - \mu\nabla q)u_n + \alpha_n\mathcal{P}_{\mathcal{E}}(\mathcal{F} - \mu\nabla q)\varsigma_n, n \in \mathbb{N}, \end{aligned} \quad (39)$$

where $0 < \mu < 2/\|\mathcal{T}\|^2$. Then, $\{u_n\}$ converges weakly to a solution of SFP.

Proof. Since $\mathcal{T} := \mathcal{P}_{\mathcal{E}}(\mathcal{F} - \mu\nabla q)$ is nonexpansive, from Theorem 1.

Next, we prove the strong convergence results. \square

Theorem 3. Let $\{u_n\}$ be generated by (5) and $\mathcal{T} = \mathcal{P}_{\mathcal{E}}[\mathcal{F} - \gamma\mathcal{A}^*(\mathcal{F} - \mathcal{P}_{\mathcal{Q}})\mathcal{A}]$. Then, $\{u_n\}$ converges strongly to a point in Ω if and only if $\liminf_{n \rightarrow \infty} d(u_n, \Omega) = 0$.

Proof. If the sequence $\{u_n\}$ has a strong convergence to a point in Ω , then it follows that $\liminf_{n \rightarrow \infty} d(u_n, \Omega) = 0$. To get to the converse, suppose that $\liminf_{n \rightarrow \infty} d(u_n, \Omega) = 0$. Since $F(\mathcal{T}) = \Omega \neq \emptyset$. It follows that $\liminf_{n \rightarrow \infty} d(u_n, F(\mathcal{T})) = 0$. Let $u^* \in F(\mathcal{T})$. Using Lemma 5, we have $\lim_{n \rightarrow \infty} \|u_n - u^*\|$ exists. Thus, $\lim_{n \rightarrow \infty} d(u_n, F(\mathcal{T}))$ exists and $\lim_{n \rightarrow \infty} d(u_n, F(\mathcal{T})) = 0$.

Next, we show that $\{u_n\}$ is a Cauchy sequence in \mathcal{E} . Since $\lim_{n \rightarrow \infty} d(u_n, F(\mathcal{T})) = 0$, given $\varepsilon > 0$, there exists a natural number n_0 such that for all $n \geq n_0$, $d(u_n, F(\mathcal{T})) < \varepsilon/2$. Meanwhile,

$$\inf \left\{ \|u_{n_0} - u^*\| : u^* \in F(\mathcal{T}) \right\} < \frac{\varepsilon}{2}. \quad (40)$$

So, we can find $v^* \in F(\mathcal{T})$ such that $\|u_{n_0} - v^*\| < \varepsilon/2$. For $n \geq n_0$ and $m \geq 1$, we have

$$\begin{aligned} \|u_{n+m} - u_n\| &\leq \|u_{n+m} - v^*\| + \|u_n - v^*\| \\ &\leq \|u_{n_0} - v^*\| + \|u_{n_0} - v^*\| \\ &< \frac{\varepsilon}{2} + \frac{\varepsilon}{2} = \varepsilon. \end{aligned} \quad (41)$$

This shows that $\{u_n\}$ is a Cauchy sequence in \mathcal{E} . From \mathcal{E} is a closed subset in \mathcal{H} . Then, there exists $\xi \in \mathcal{E}$ such that $\lim_{n \rightarrow \infty} u_n = \xi$. Now $\lim_{n \rightarrow \infty} d(u_n, F(\mathcal{T})) = 0$ gives that $d(\xi, F(\mathcal{T})) = 0$. Note that $F(\mathcal{T})$ is closed. Therefore, $\xi \in F(\mathcal{T})$. Again, using $F(\mathcal{T}) = \Omega$, we have $\xi \in \Omega$. Thus, $\{u_n\}$ converges to a point in Ω . This completes the proof.

A mapping \mathcal{T} satisfy Condition A (see [33]) if there exists a nondecreasing function $f: [0, +\infty) \rightarrow [0, +\infty)$ with $f(0) = 0$ and $f(r) > 0$ for all $r \in (0, +\infty)$ such that

$$\|u - \mathcal{T}u\| \geq f(d(u, F(\mathcal{T}))), \quad (42)$$

for all $u \in \mathcal{E}$.

Next, we can prove strong convergence of (5) under Condition A, which is weaker than the compactness of the mappings' domain. \square

Theorem 4. If \mathcal{T} satisfies Condition A, then the sequence $\{u_n\}$ defined by (5) converges strongly to a point in Ω .

Proof. Using Lemma 6, we also get

$$\lim_{n \rightarrow \infty} \|u_n - \mathcal{T}u_n\| = 0. \quad (43)$$

Since \mathcal{T} is a given, it follows that

$$\lim_{n \rightarrow \infty} f(d(u_n, F(\mathcal{T}))) \leq \lim_{n \rightarrow \infty} \|u_n - \mathcal{T}u_n\| = 0. \quad (44)$$

Now $f: [0, +\infty) \rightarrow [0, +\infty)$ with $f(0) = 0$ and $f(r) > 0$ for all $r \in (0, +\infty)$, gives that

$$\lim_{n \rightarrow \infty} d(u_n, F(\mathcal{T})) = 0, \quad (45)$$

and it follows that

$$\lim_{n \rightarrow \infty} d(u_n, \Omega) = 0. \quad (46)$$

From Theorem 3, we have $\{u_n\}$ converges strongly to a point in Ω . This completes the proof. \square

4. Numerical Examples

In this part, we study and compare numerical results of the proposed algorithm (5) with the Dang algorithm (4) to declare that the proposed algorithm is more effective.

Example 1. Suppose that $\mathcal{H}_1 = \mathcal{H}_2 = \mathbb{R}^3$, $\mathcal{C} = \{u \in \mathbb{R}^3: \|u\| \leq 1\}$, $\mathcal{Q} = \{u \in \mathbb{R}^3: \|u\| \leq 2\}$, and $\mathcal{T}u = Mu$.

$$M = \begin{bmatrix} -3 & 1 & 2 \\ -1 & 0 & 1 \\ 1 & 2 & -1 \end{bmatrix}, \quad (47)$$

and take an initial point $u_0 = \{0.6, 0.5, 1.1\}$.

Example 2. Suppose that $\mathcal{H}_1 = \mathcal{H}_2 = \mathbb{R}^3$, $\mathcal{C} = \{u \in \mathbb{R}^3: \|u\| \leq 1\}$, $\mathcal{Q} = \{u \in \mathbb{R}^3: \|u\| \leq 2\}$, and $\mathcal{T}u = Mu$.

$$M = \begin{bmatrix} 2 & -1 & 0 \\ -1 & 2 & -1 \\ 0 & -1 & 2 \end{bmatrix}, \quad (48)$$

and take an initial point $u_0 = \{1.2, 0.6, 0.4\}$.

The projections $\mathcal{P}_{\mathcal{C}}$ and $\mathcal{P}_{\mathcal{Q}}$ of u onto sets \mathcal{C} and \mathcal{Q} are as follows:

$$\mathcal{P}_{\mathcal{C}}(u) = \begin{cases} u, & \|u\| \leq 1, \\ \frac{u}{\|u\|}, & \|u\| \geq 1, \end{cases} \quad (49)$$

$$\mathcal{P}_{\mathcal{Q}}(u) = \begin{cases} u, & \|u\| \leq 2, \\ \frac{u}{\|u\|}, & \|u\| \geq 2. \end{cases}$$

Meanwhile, choose

$$\begin{aligned} \alpha_n &= \beta_n \\ &= \gamma_n \\ &= \frac{n}{n+1} \\ &= 0.99 \quad \text{and} \end{aligned} \quad (50)$$

$$\lambda_n = \frac{1}{\|\mathcal{A}\|_2^2},$$

for Dang and proposed methods. We take $\|u_{n+1} - u_n\| < 10^{-15}$ as the standard of stopping in the process of calculation. All codes were written in MATLAB 2019b. By computing, we obtain the iteration steps and CPU time of these three comparing algorithms in converging to the solution of Examples 1 and 2 as shown in Table 1.

Tables 2 and 3 show the convergence of comparing sequences of Examples 1 and 2 generated by Dang and proposed methods. It can be found from the computing results of Tables 1–3 that, under the same conditions, the results of the proposed method are highly effective compared with Dang method.

5. Applications

This section is devoted to some applications by using the proposed algorithm (5).

5.1. Image Restoration Problems. Assume that B is a matrix with \tilde{m} rows and \tilde{n} columns that represents the degraded representation of the true image X . The restoration model can be obtained by stacking the columns of B and X into two long vectors, \mathbf{b} and \mathbf{u} , both of which have lengths of $n = \tilde{m}\tilde{n}$. The following linear equation system may be used to describe the restoration model as a one-dimensional vector:

$$\mathbf{b} = M\mathbf{u}, \quad (51)$$

where the true image is represented by $\mathbf{u} \in \mathbb{R}^n$, the observed image is represented by $\mathbf{b} \in \mathbb{R}^n$, and the blurring matrix is represented by $M \in \mathbb{R}^{n \times n}$.

Issue (52) is a least squares (LS) problem that needs to be resolved in order to resemble the true image on the restoration model (51).

$$\min_{\mathbf{u}} \frac{1}{2} \|\mathbf{b} - M\mathbf{u}\|_2^2. \quad (52)$$

We will use our key findings for resolving the restoration model (51) by setting the following by using $q(\mathbf{u})$ as above equation. And the following methods are used to resolve the image restoration problem.:

$$\begin{aligned} \mathbf{z}_n &= (1 - \gamma_n)\mathbf{u}_n + \gamma_n(\mathbf{u}_n - \mu M^T(M\mathbf{u}_n - \mathbf{b})), \\ \mathbf{y}_n &= (1 - \beta_n)\mathbf{z}_n + \beta_n(\mathbf{z}_n - \mu M^T(M\mathbf{z}_n - \mathbf{b})), \\ \mathbf{u}_{n+1} &= (1 - \alpha_n)(\mathbf{u}_n - \mu M^T(M\mathbf{u}_n - \mathbf{b})) \\ &\quad + \alpha_n(\mathbf{y}_n - \mu M^T(M\mathbf{y}_n - \mathbf{b})). \end{aligned} \quad (53)$$

The problem (51) is solved using (53), using the parameter (50) and $\mu = 1/\|M^T M\|_2$.

To illustrate the viability of the suggested algorithm, the true RGB (color image) is presented in Figure 1. Peak signal-to-noise ratio (PSNR) is a quantitative metric that is used to assess how well the contrasting algorithms at \mathbf{u}_n work during the image deblurring process. Moreover, we employ the following formula:

$$\frac{\|\mathbf{u}_n - \mathbf{u}\|_{\infty}}{\|\mathbf{u}\|_{\infty}}, \quad (54)$$

to measure the figure error, which is called the relative figure norm.

We then show how to restore photos that have been damaged by the matrices M_G (Gaussian blur of filter size 9×9 with standard deviation $\sigma = 4$), M_O (out focus

TABLE 1: Iteration steps and CPU time of the Dang method (4) and proposed method (5) for the numerical experiment of Examples 1 and 2.

Algorithm	Iterations number		CPU time (sec)	
	Example 1	Example 2	Example 1	Example 2
Dang (4)	111	112	$7.973e-04$	$9.648e-04$
Proposed (5)	2	2	$3.985e-04$	$4.091e-04$

TABLE 2: Comparative sequences of the Dang method (4) and proposed method (5) for the numerical experiment of Example 1 with three decimal places.

Iteration number	Example 1	
	Dang (4)	Proposed (5)
1	(0.600, 0.500, 1.100)	(0.600, 0.500, 1.100)
2	(0.561, 0.467, 1.028)	(0.444, 0.370, 0.815)
3	(0.534, 0.445, 0.979)	
4	(0.514, 0.428, 0.943)	
5	(0.499, 0.416, 0.915)	
⋮	⋮	
29	(0.444, 0.370, 0.815)	
⋮	⋮	
111	(0.444, 0.370, 0.815)	

TABLE 3: Comparative sequences of the Dang method (4) and proposed method (5) for the numerical experiment of Example 2 with three decimal places.

Iteration number	Example 2	
	Dang (4)	Proposed (5)
1	(1.200, 0.600, 0.400)	(1.200, 0.600, 0.400)
2	(1.117, 0.557, 0.979)	(0.857, 0.428, 0.285)
3	(1.054, 0.527, 0.943)	
4	(1.010, 0.505, 0.915)	
5	(0.977, 0.488, 0.815)	
⋮	⋮	
28	(0.857, 0.428, 0.285)	
⋮	⋮	
112	(0.857, 0.428, 0.285)	

blur with radius $r = 6$), and M_M (motion blur specifying with 21 pixels of motion length) (see Figure 2). The reconstructed RGB image shown in Figures 3–5 employs three blurring matrices M_G, M_O , and M_M for 50^{th} , $1,000^{th}$, and $20,000^{th}$ iterations to address the restoration problem. These figures show that the quality of restored images utilizing (53) for solving (51) improve for the three types of degraded images.

Additionally, employing the suggested algorithms with $100,000^{th}$ iterations, the behavior of the relative figure error and the PSNR quality of the deteriorated RGB image are exhibited.

It is interesting to note that the relative errors plot of the suggested technique decreases with the number of iterations. As the number of iterations increases, their graphs also grow, according to the PSNR plots in Figure 6. It can be said that the suggested approach improves the quality of the three distinct types of real RGB images.



FIGURE 1: True images ($243 \times 349 \times 3$).

5.2. *Signal Recovering Problems.* Compressed sensing can be defined in signal processing given by

$$\mathbf{y} = \mathbf{A}\mathbf{u} + \nu, \quad (55)$$

where $\mathbf{u} \in \mathbb{R}^n$ is the original signal, ν is the noise, $\mathbf{y} \in \mathbb{R}^m$ is the observed signal with noisy, and $A \in \mathbb{R}^{m \times n}$ is a degraded matrix. Solving the LASSO problem, (56) can be thought of as finding solutions to previously determined linear equation systems.

$$\min_{\mathbf{u} \in \mathbb{R}^n} \frac{1}{2} \|\mathbf{y} - \mathbf{A}\mathbf{u}\|_2^2 \quad \text{subject to } \|\mathbf{u}\|_1 \leq t, \quad (56)$$

where $t > 0$ is a given constant. We can use our strategy to solve the issue (56) by putting $\mathcal{T} = \mathcal{P}_{\mathcal{C}}(\mathcal{I} - \mu \nabla q)$, where $q(\mathbf{u}) = \frac{1}{2} \|\mathbf{y} - \mathbf{A}\mathbf{u}\|_2^2$ and $\nabla q(\mathbf{u}) = A^T (\mathbf{A}\mathbf{u} - \mathbf{y})$. We demonstrate how to use our approach in signal recovery issues (55). Let $\{\mathbf{u}_n\}$ generated by $C = \{\mathbf{u} \in \mathbb{R}^n: \|\mathbf{u}\|_1 \leq t\}$, we acquire techniques for solving

$$\begin{aligned} \mathbf{w}_n &= (1 - \gamma_n)\mathbf{u}_n + \gamma_n \mathcal{T} \mathbf{u}_n, \\ \mathbf{z}_n &= (1 - \beta_n)\mathbf{w}_n + \beta_n \mathcal{T} \mathbf{w}_n, \\ \mathbf{u}_{n+1} &= (1 - \alpha_n)\mathcal{T} \mathbf{u}_n + \alpha_n \mathcal{T} \mathbf{z}_n, \end{aligned} \quad (57)$$

where $\mu \in (0, 2/\|A^T A\|_2)$ and $\alpha_n, \beta_n, \gamma_n \in (0, 1), \forall n \in \mathbb{N}$.

Following that, various experiments are shown to demonstrate the convergence and usefulness of algorithm (50). $\mathbf{y}_i = A_i \mathbf{u} + \nu_i, i = 1, 2, 3$ with $m = 512$ is generated by \mathbf{u} with $n = 1024$ formed by the uniform distribution in the range $[-2, 2]$ with 70 nonzero items. The original signal is shown in Figure 7.

The procedure begins when the begin data \mathbf{u}_0 with $n = 1024$ is chosen at random and t is the number of nonzero elements (see Figure 8).

The observation signal \mathbf{y}_i is shown in Figure 9.

A_i formed by the normal distribution with mean of zero and variance of one and white Gaussian noise $\nu_i, i = 1, 2, 3$ (see Figure 10).

The convergence features of algorithm (57) with the permutation of the blurring matrices A_1, A_2 , and A_3 are illustrated and analyzed. The relative inaccuracy is calculated by using $\|\mathbf{u}_n - \mathbf{u}_2\|/\|\mathbf{u}_2\|$. The signal-to-noise ratio (SNR) is used to quantify the performance of the recovered signal at the n^{th} iteration (SNR). In addition, the comparative



FIGURE 2: True images are blurred by matrices M_G , M_O , and M_M respectively.



FIGURE 3: Rebuilt images degraded by blurred matrices M_G being 50th, 1,000th, and 20,000th used iterations.



FIGURE 4: Rebuilt images degraded by blurred matrices M_O being 50th, 1,000th, and 20,000th used iterations.



FIGURE 5: Rebuilt images degraded by blurred matrices M_M being 50th, 1,000th, and 20,000th used iterations.

algorithms' parameters α_n, β_n , and γ_n are set to the default parameter (50).

Figure 11 depicts the behavior of relative signal error and SNR quality of the proposed approach with the blurring matrices A_1, A_2 , and A_3 .

The relative signal error plot reduces until it converges to some fixed value, which is impressive. The SNR quality plot of the provided approach shows that the SNR value grows until it also converges to a constant number.

Figures 12–14 demonstrate the recovered signal using the proposed techniques with the group of operator and noise A_i and $\nu_i, i = 1, 2, 3$. The improvement of SNR quality for the recovering signals based on 5,000th, 10,000th, and 20,000th number of iterations are also shown on these figures. As illustrated in Figures 12–14, the proposed algorithms (57) to solve the signal recovery problem have been shown to improve the quality of recovered signals for three different types of degraded signals.

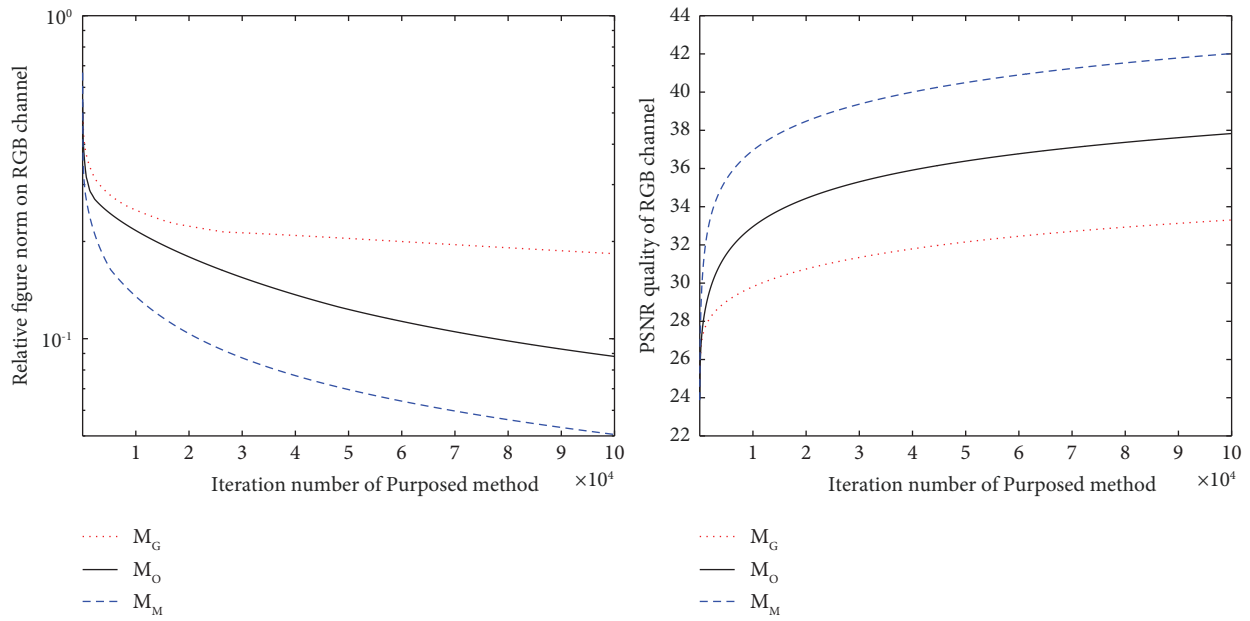


FIGURE 6: The relative figures norm and PSNR plots of the proposed method for all degraded RGB images.

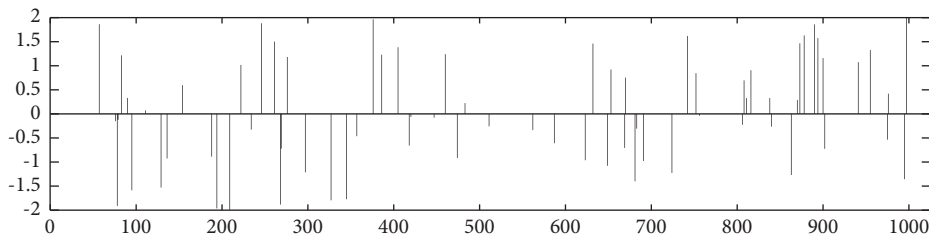


FIGURE 7: The original signal contains 70 nonzero components.

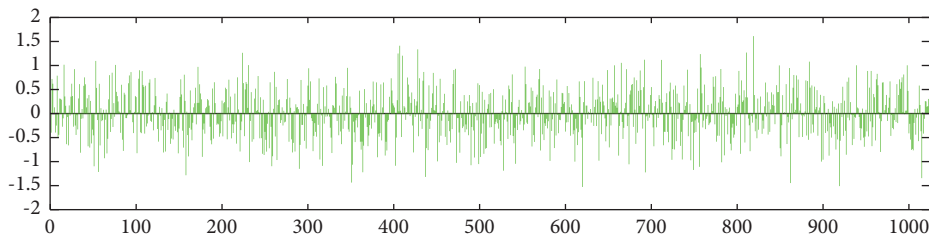


FIGURE 8: Initial signals \mathbf{u}_0 .

5.3. *Polynomiography.* In 2005, polynomiography is defined by Kalantari (see, e.g. [34–40]). The formula for Newton’s method of calculating the roots of a complex polynomial P is as follows:

$$z_{n+1} = z_n - \frac{p(z_n)}{p'(z_n)}, n = 0, 1, 2, \dots, \tag{58}$$

where $z_0 \in \mathbb{C}$ is an initial point. Here, we have (59) by using (58). Consider a Hilbert space $\mathcal{H} = \mathbb{C}$, $v_0 = (x_0, y_0)$, and $\{\alpha_n\}, \{\beta_n\}, \{\gamma_n\} \subset (0, 1)$. The following formula generates polynomiographs:

$$\begin{aligned} w_n &= (1 - \gamma_n)v_n + \gamma_n \left(v_n - \frac{p(v_n)}{p'(v_n)} \right), \\ z_n &= (1 - \beta_n)w_n + \beta_n \left(w_n - \frac{p(w_n)}{p'(w_n)} \right), \\ v_{n+1} &= (1 - \alpha_n) \left(v_n - \frac{p(v_n)}{p'(v_n)} \right) + \alpha_n \left(z_n - \frac{p(z_n)}{p'(z_n)} \right), \end{aligned} \tag{59}$$

where $\{\alpha_n\}, \{\beta_n\}, \{\gamma_n\}$ are real sequences in $(0, 1)$.

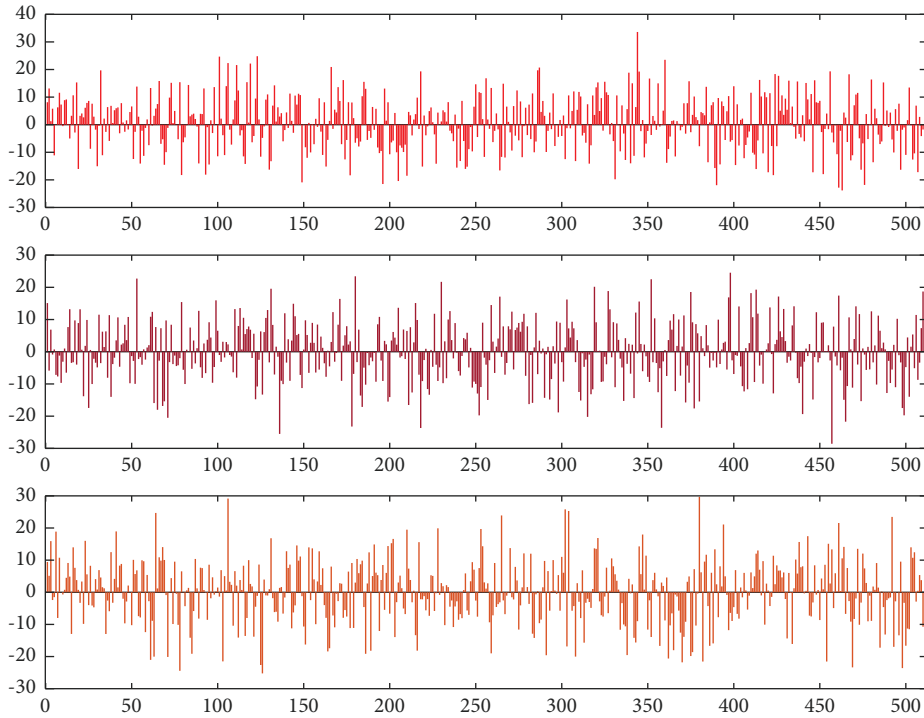


FIGURE 9: Degraded signals y_1 , y_2 , and y_3 .

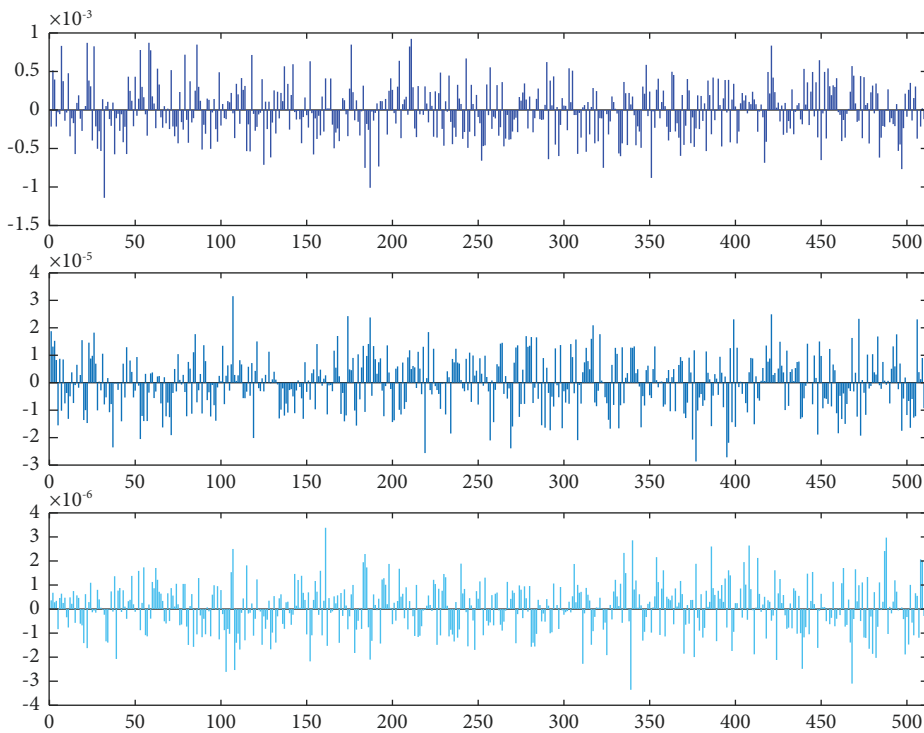


FIGURE 10: Noise signals v_1 , v_2 , and v_3 .

This subsection shows some examples of the polynomiographs obtained by using (59) with real and complex-valued parameters using different color maps.

5.3.1. *Polynomiographs with Real-Valued Parameters of Iterations.* Polynomiographs for complex polynomial equation $p_1(z) = z^3 - 3z^2 + 1$ and $p_2(z) = z^4 + z^2 - 1$ are

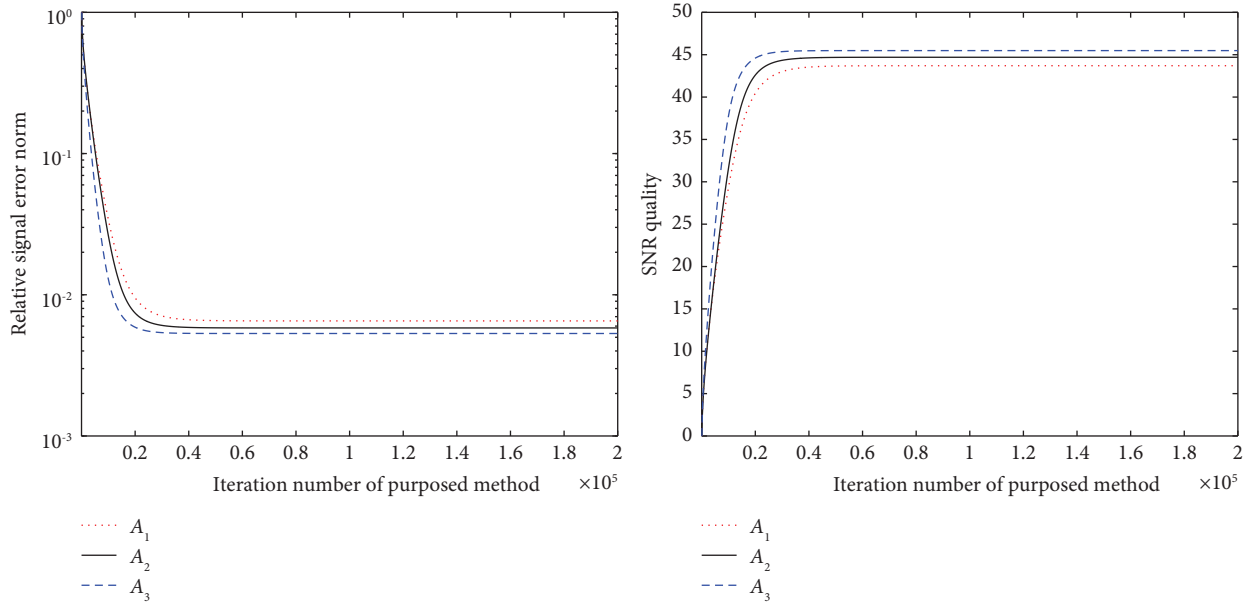


FIGURE 11: The relative signal error and SNR plots of the proposed algorithm with the blurring matrices $A_1, A_2,$ and A_3 in recovering the observed signal with 200,000th iterations.

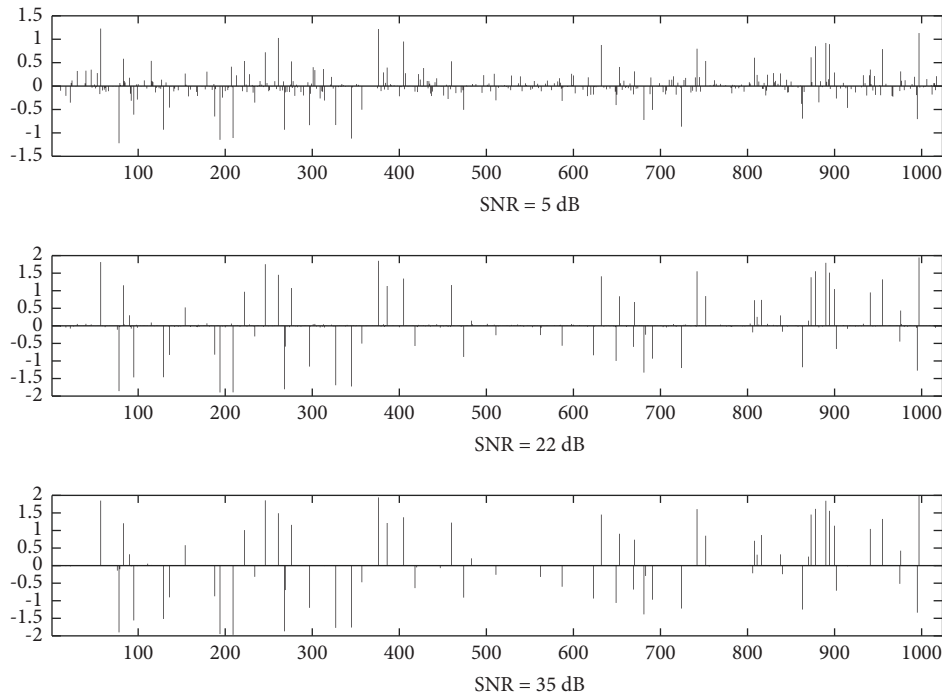


FIGURE 12: Recovering signals based on the SNR quality for the degraded signal with operator A_1 and noise γ_1 .

presented in Figures 15 and 16, respectively. Polynomiographs were generated by resolution 500×500 pixels, number of iterations $n = 15$, accuracy $\epsilon = 0.001$, and $A = [2, 2]^2$. The following parameters were fixed in the iterations: $\alpha_n = 0.35$, $\beta_n = 0.65$, and $\gamma = 0.55$.

5.3.2. Polynomiographs with Complex-Valued Parameters of Iterations. Polynomiographs for complex polynomial

equations, $p_1(z) = z^3 - 3z^2 + 1$ and $p_2(z) = z^4 + z^2 - 1$, are presented in Figures 17 and 18, respectively. Polynomiographs were generated by resolution 500×500 pixels, number of iterations $n = 15$, accuracy $\epsilon = 0.001$, and $A = [2, 2]^2$. The following parameters were fixed in the iterations: $\alpha_n = 0.35 + 0.3i$, $\beta_n = 0.65 + 0.4i$, and $\gamma = 0.55 + 0.75i$.

Figures 15 and 16 show how real parameter components affect symmetry, whereas Figures 17 and 18 show how

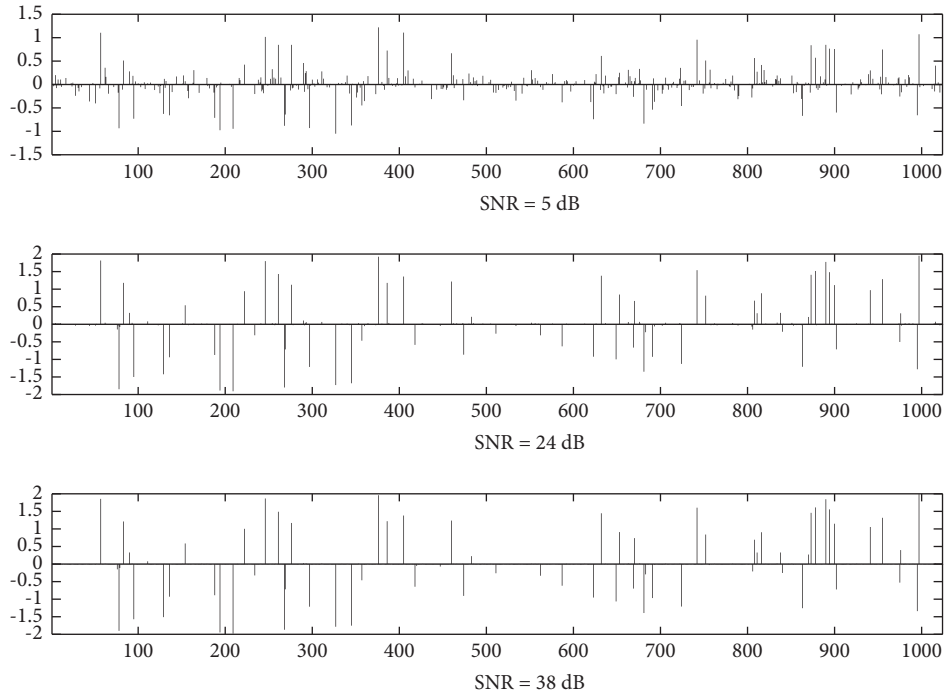


FIGURE 13: Recovering signals based on the SNR quality for the degraded signal with operator A_2 and noise ν_2 .

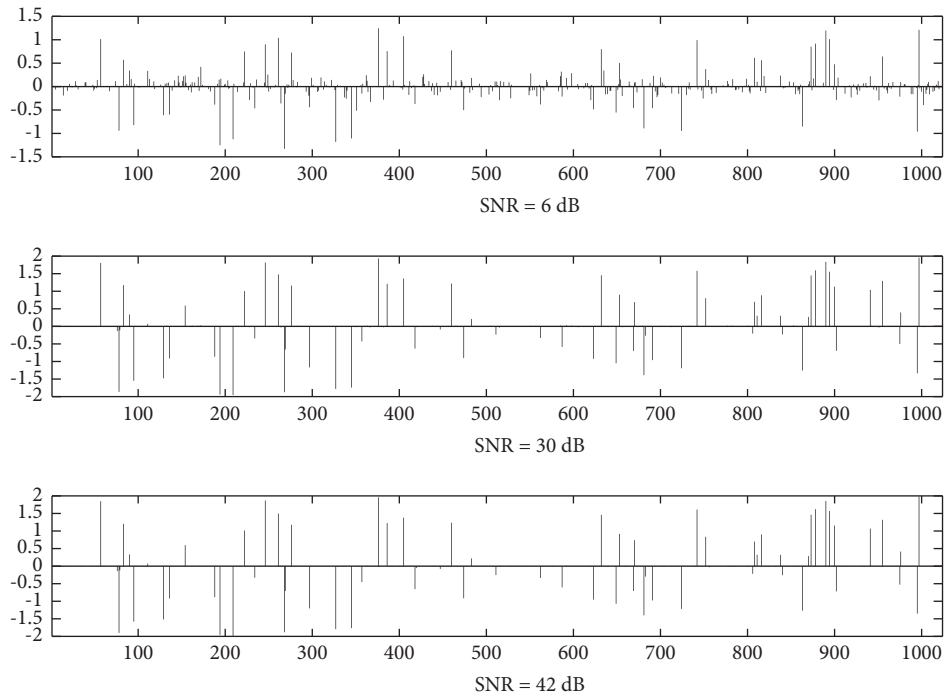


FIGURE 14: Recovering signals based on the SNR quality for the degraded signal with operator A_3 and noise ν_3 .

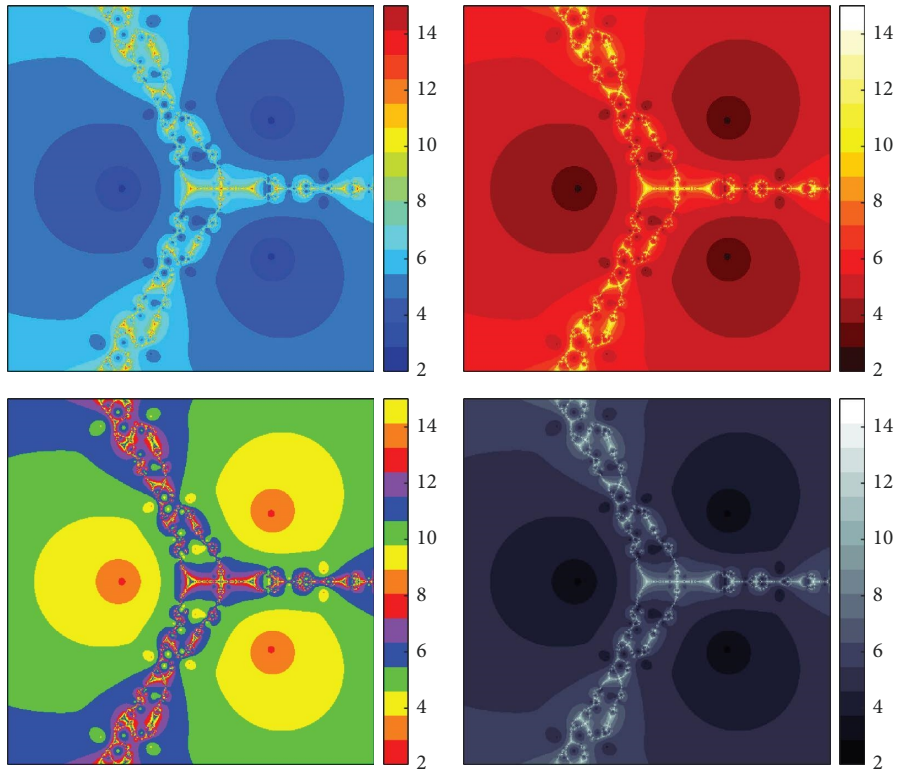


FIGURE 15: Examples of polynomiographs of different color maps for p_1 with real-valued parameters of (59).

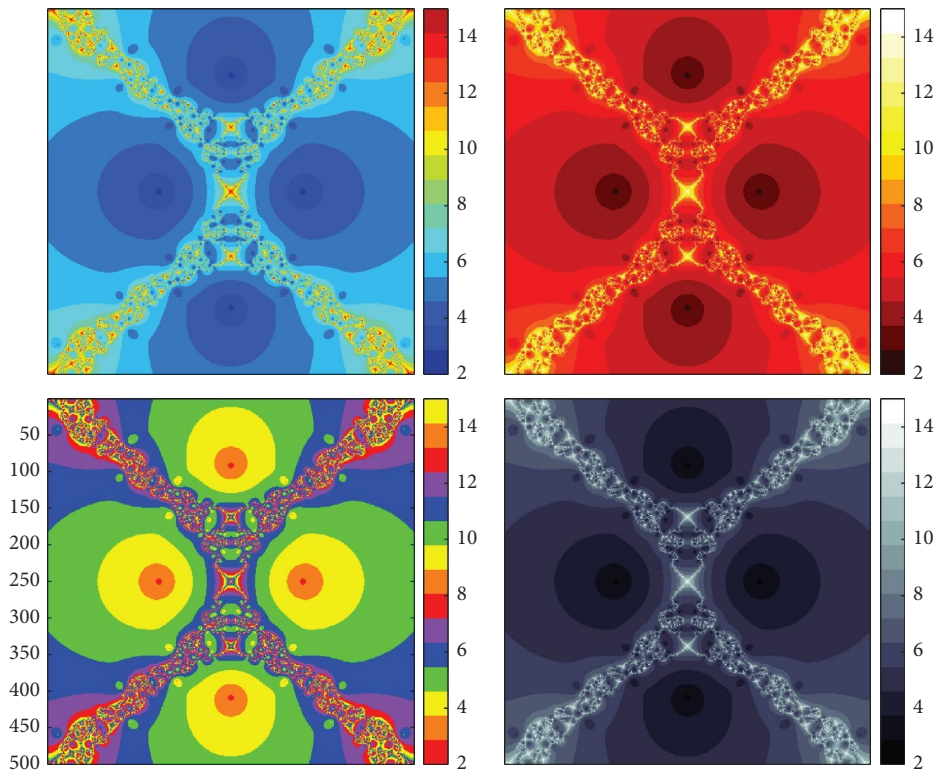


FIGURE 16: Examples of polynomiographs of different color maps for p_2 with real-valued parameters of (59).

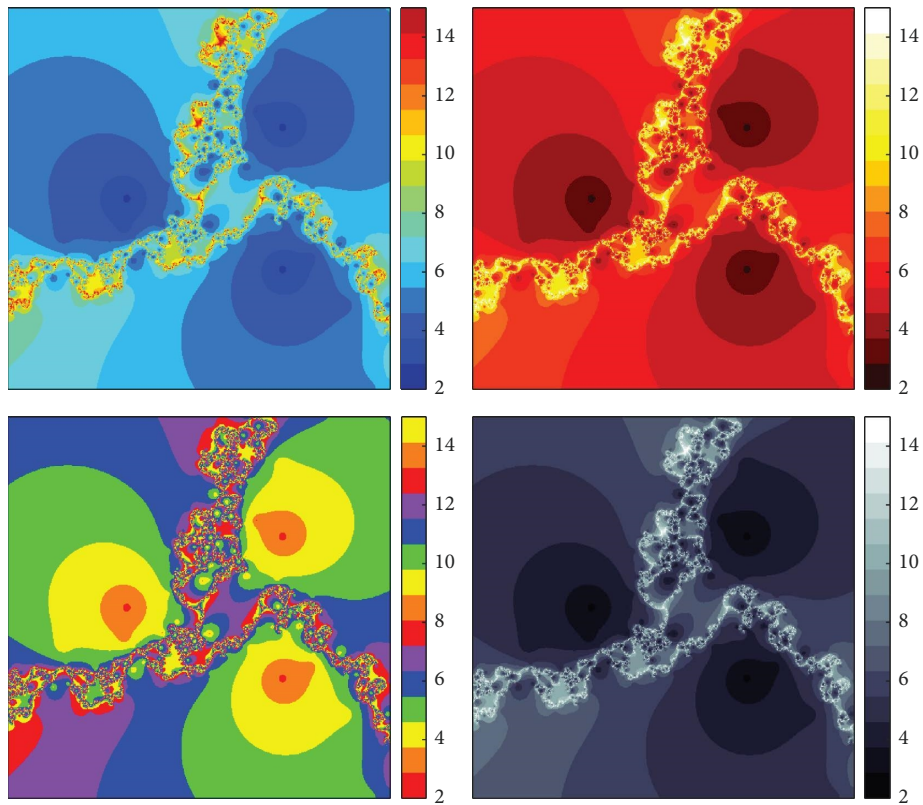


FIGURE 17: Examples of polynomiographs of different color maps for p_1 with complex-valued parameters of (59).

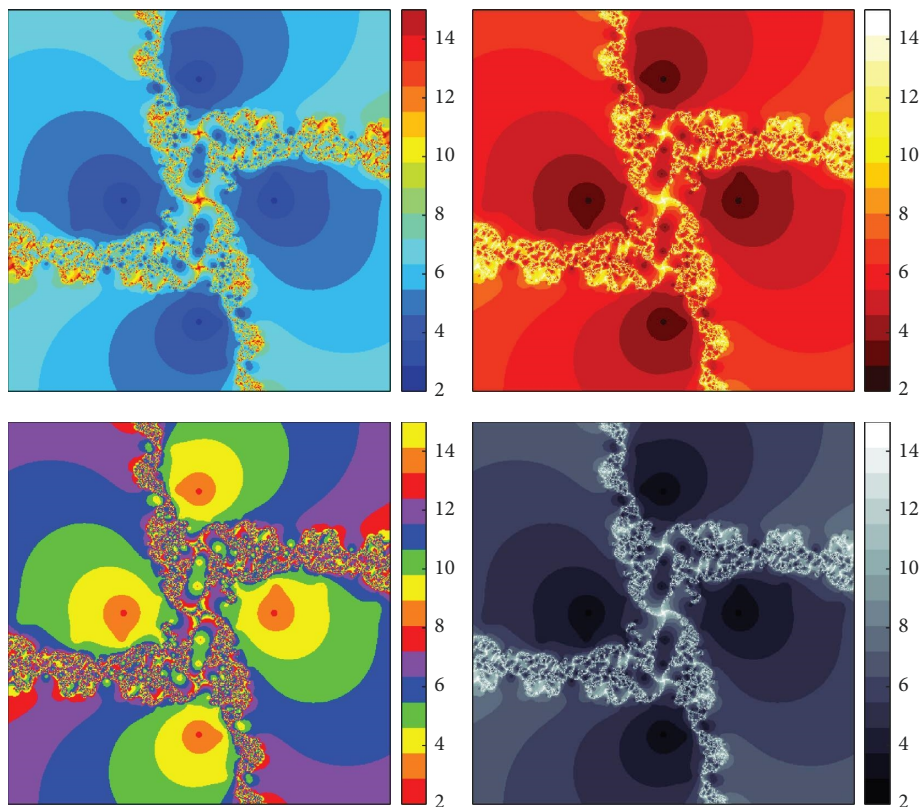


FIGURE 18: Examples of polynomiographs of different color maps for p_2 with complex-valued parameters of (59).

imaginary parameter components produce asymmetric twisting of the polynomiographs and affect the statics or dynamics of the pictures.

Data Availability

No data were used in this manuscript.

Conflicts of Interest

The authors declare that they have no conflicts of interest.

Acknowledgments

The first author acknowledges the financial support provided by the International SciKU Branding (ISB), Faculty of Science, Kasetsart University. C. Chairatsiripong would like to thank the revenue budget for 2021 (PBTSC64001), School of Science, University of Phayao. T. Thianwan would like to thank the Thailand Science Research and Innovation Fund, and University of Phayao (Grant nos. FF65-RIM072 and FF66-UoE015).

References

- [1] Y. Censor and T. Elfving, "A multiprojection algorithm using Bregman projections in a product space," *Numerical Algorithms*, vol. 8, no. 2-4, pp. 221-239, 1994.
- [2] H. He, C. Ling, and H. K. Xu, "An implementable splitting algorithm for the l_1 -norm regularized split feasibility problem," *Journal of Scientific Computing*, vol. 67, pp. 281-298, 2015.
- [3] D. A. Lorenz, F. Sch, S. Wenger, and S. Wenger, "The linearized Bregman method via split feasibility problems: analysis and generalizations," *SIAM Journal on Imaging Sciences*, vol. 7, no. 2, pp. 1237-1262, 2014.
- [4] Y. Censor, T. Elfving, N. Kopf, and T. Bortfeld, "The multiple-sets split feasibility problem and its applications for inverse problems," *Inverse Problems*, vol. 21, no. 6, pp. 2071-2084, 2005.
- [5] Y. Censor, T. Bortfeld, B. Martin, and A. Trofimov, "A unified approach for inversion problems in intensity-modulated radiation therapy," *Physics in Medicine and Biology*, vol. 51, no. 10, pp. 2353-2365, 2006.
- [6] C. Byrne, "A unified treatment of some iterative algorithms in signal processing and image reconstruction," *Inverse Problems*, vol. 20, no. 1, pp. 103-120, 2004.
- [7] C. Byrne, "Iterative oblique projection onto convex sets and the split feasibility problem," *Inverse Problems*, vol. 18, no. 2, pp. 441-453, 2002.
- [8] B. Qu and N. Xiu, "A note on the CQ algorithm for the split feasibility problem," *Inverse Problems*, vol. 21, no. 5, pp. 1655-1665, 2005.
- [9] Q. Yang, "The relaxed CQ algorithm solving the split feasibility problem," *Inverse Problems*, vol. 20, no. 4, pp. 1261-1266, 2004.
- [10] J. Zhao and Q. Yang, "Several solution methods for the split feasibility problem," *Inverse Problems*, vol. 21, no. 5, pp. 1791-1799, 2005.
- [11] H. K. Xu, "Iterative methods for the split feasibility problem in infinite-dimensional Hilbert spaces," *Inverse Problems*, vol. 26, no. 10, Article ID 105018, 2010.
- [12] H. K. Xu, "A variable Krasnosel'skiĭ-Mann algorithm and the multiple-set split feasibility problem," *Inverse Problems*, vol. 22, no. 6, pp. 2021-2034, 2006.
- [13] H. H. Bauschke and J. M. Borwein, "On projection algorithms for solving convex feasibility problem," *SIAM Review*, vol. 38, pp. 367-426, 1996.
- [14] G. Lopez, V. Martín, F. Wang, and H. K. Xu, "Solving the split feasibility problem without prior knowledge of matrix norms," *Inverse Problems*, vol. 28, Article ID 085004, 2012.
- [15] A. Bnouhachem, M. A. Noor, M. Khalfaoui, and S. Zhaohan, "On descent projection method for solving the split feasibility problems," *Journal of Global Optimization*, vol. 54, no. 3, pp. 627-639, 2012.
- [16] H. Zhou and P. Wang, "Adaptively relaxed algorithms for solving the split feasibility problem with a new step size," *Journal of Inequalities and Applications*, vol. 2014, no. 1, 2014.
- [17] H. Cui and F. Wang, "Iterative methods for the split common fixed point problem in Hilbert spaces," *Journal of Fixed Point Theory and Applications*, vol. 2014, no. 1, 2014.
- [18] C. Byrne, Y. Censor, A. Gibali, and S. Reich, "The split common null point problem," *Journal of Nonlinear and Convex Analysis*, vol. 13, pp. 759-775, 2012.
- [19] E. Masad and S. Reich, "A note on the multiple-set split convex feasibility problem in Hilbert space," *Journal of Nonlinear and Convex Analysis*, vol. 8, pp. 367-371, 2007.
- [20] Q. L. Dong, L. Liu, and Y. Yao, "Self-adaptive projection and contraction methods with alternated inertial terms for solving the split feasibility problem," *Journal of Nonlinear and Convex Analysis*, vol. 23, pp. 591-605, 2022.
- [21] K. Saechou and A. Kangtunyakarn, "The method for solving the extension of general of the split feasibility problem and fixed point problem of the cutter," *Journal of Inequalities and Applications*, vol. 2022, no. 1, 2022.
- [22] F. G. Gao, X. X. Liu, and X. C. Li, "Strong Convergence on the Split Feasibility Problem by Mixing w-Mapping," *Journal of Mathematics*, vol. 2021, Article ID 9924937, 6 pages, 2021.
- [23] M. A. Noor, "New approximation schemes for general variational inequalities," *Journal of Mathematical Analysis and Applications*, vol. 251, no. 1, pp. 217-229, 2000.
- [24] R. Glowinski and P. L. Tallec, *Augmented Lagrangian and Operator-Splitting Methods in Nonlinear Mechanics*, SIAM, PA, USA, 1989.
- [25] S. Haubruge, V. H. Nguyen, and J. J. Strodiot, "Convergence analysis and applications of the Glowinski Le Tallec splitting method for finding a zero of the sum of two maximal monotone operators," *Journal of Optimization Theory and Applications*, vol. 97, no. 3, pp. 645-673, 1998.
- [26] D. Yambangwai and T. Thianwan, "Convergence point of G-nonexpansive mappings in Banach spaces endowed with graphs applicable in image deblurring and signal recovering problems," *Ricerche di Matematica*, vol. 2021, pp. 1-28, 2021.
- [27] Y. Z. Dang and Y. Gao, "The strong convergence of a three-step algorithm for the split feasibility problem," *Optimization Letters*, vol. 7, no. 6, pp. 1325-1339, 2013.
- [28] B. S. Thakur, D. Thakur, and M. Postolache, "A new iteration scheme for approximating fixed Points of nonexpensive mapping," *Faculty of Sciences and Math*, vol. 10, pp. 2711-2720, 2016.
- [29] M. Feng, L. Shi, and R. Chen, "A new three-step iterative algorithm for solving the split feasibility problem," *UPB Scientific Bulletin, Series A*, vol. 81, no. 1, pp. 93-102, 2019.
- [30] Z. Opial, "Weak convergence of the sequence of successive approximations for nonexpansive mappings," *Bulletin of the*

- American Mathematical Society*, vol. 73, no. 4, pp. 591–597, 1967.
- [31] J. Schu, “Weak and strong convergence to fixed points of asymptotically nonexpansive mappings,” *Bulletin of the Australian Mathematical Society*, vol. 43, no. 1, pp. 153–159, 1991.
- [32] J. P. Aubin and A. Cellina, *Differential Inclusions: Set-Valued Maps and Viability Theory*, Springer, Berlin, Germany, 1984.
- [33] H. F. Senter and W. G. Dotson, “Approximating fixed points of nonexpansive mappings,” *Proceedings of the American Mathematical Society*, vol. 44, no. 2, pp. 375–380, 1974.
- [34] B. Kalantari, “Method of creating graphical works based on polynomials,” Academic Publications, Ltd, Yorkshire, UK, Patent, US6894705, 2005.
- [35] B. Kalantari, *Polynomial Root-Finding and Polynomiography*, World Scientific Publishing Co. Pte. Ltd, New Jersey, NJ, USA, 2009.
- [36] B. B. Mandelbrot, *The Fractal Geometry of Nature*, W. H. Freeman, New York, NY, USA, 1982.
- [37] Y. C. Kwun, M. Tanveer, W. Nazeer, K. Gdawiec, and S. M. Kang, “Mandelbrot and julia sets via jungck–CR iteration with S -convexity,” *IEEE Access*, vol. 7, pp. 12167–12176, 2019.
- [38] Y. C. Kwun, M. Tanveer, W. Nazeer, M. Abbas, and S. M. Kang, “Fractal generation in modified Jungck–S orbit,” *IEEE Access*, vol. 7, pp. 35060–35071, 2019.
- [39] H. Qi, M. Tanveer, W. Nazeer, and Y. Chu, “Fixed point results for fractal generation of complex polynomials involving sine function via non–standard iterations,” *IEEE Access*, vol. 8, pp. 154301–154317, 2020.
- [40] Y. C. Kwun, A. A. Shahid, W. Nazeer, M. Abbas, and S. M. Kang, “Fractal generation via CR iteration scheme with S -convexity,” *IEEE Access*, vol. 7, pp. 69986–69997, 2019.